INVITED PAPER

Ultralow Power Circuit Design for Wireless Sensor Nodes for Structural Health Monitoring

This paper presents state-of-the-art ultralow power digital circuits for future generations of wireless sensors reliant on power harvesting.

By Yoonmyung Lee, *Member IEEE*, David Blaauw, *Fellow IEEE*, and Dennis Sylvester, *Fellow IEEE*

ABSTRACT | Wireless sensor nodes (WSNs) are essential elements for today's structural health monitoring (SHM). As the design technology for WSNs evolves, there have been continuous efforts to address challenges for WSNs such as short lifetime, high power consumption, and bulky volume. Recent trends show energy harvesting becoming a popular solution for extending the lifetime of WSNs; even implementing energy-autonomous systems is an option. Smaller WSN form factors have been developed for volume-limited applications and sensor nodes as small as a few mm^3 were created with custom-designed integrated circuits (ICs). Custom IC-based sensor nodes enable energy-efficient implementation of WSNs for SHM. Ultralow power circuits with operation power on the order of nanowatts are introduced in this paper. Ultralow power energy harvesters, timers, wakeup receivers, sensing modalities, and microprocessors are expected to significantly extend sensor node lifetime or achieve sensor node operation with ambient energy harvesting.

KEYWORDS | Energy harvesting; low-power electronics; sensor systems; structural engineering

I. INTRODUCTION

Complex engineering structures are a vital part of today's societies. Without civil, mechanical, and aerospace infrastructure, a society cannot maintain a high quality of modern human life. Structural health monitoring (SHM) is the process of detecting damage in these engineering structures. Damage can accumulate over a long time from daily use or it can be caused by sudden natural disasters. By detecting damage early on, proper scheduled maintenance can repair damage with minimal cost and prevent costly catastrophic failure. Recent advances in sensors and electronic technology enable SHM for a wide range of engineering structures, including buildings, bridges [1], roads [2], pipelines [3], dams [4], wind turbines [5], railroads [6], aircraft [7], ships [8], and spacecraft [9].

SHM systems typically function in three steps: 1) sensor measurement; 2) data processing; and 3) storage and delivery to the user. Measurement data should first be collected by sensors to perform a meaningful high-level structural health diagnosis. Some of the sensor measurements are used for direct diagnosis of structural health. For example, the measured pressure between a bolt and connecting steel beam indicates how tightly the bolt is engaged to the beam; similarly, the tension of a wire on a hanging wire bridge indicates how much weight it bears. On the other hand, some other types of measurements, such as temperature, humidity, wind velocity, and atmospheric pressure, are used for monitoring the environmental conditions that the structure has been exposed to. These data can be analyzed together to achieve a high-level structural health diagnosis and prognosis.

Raw measurement data often must be processed to generate meaningful results. For example, to examine the

Manuscript received April 5, 2015; revised November 11, 2015 and January 31, 2016; accepted March 17, 2016. Date of current version July 15, 2016. This work was supported by the Center for Integrated Smart Sensors funded by the Ministry of Science, ICT & Future Planning CISS-2012M3A6A6054193.

Y. Lee is with the Department of Semiconductor Systems Engineering, Sungkyunkwan University (SKKU), Suwon 16419, South Korea (e-mail: yoonmyung@skku.edu).
D. Blaauw and **D. Sylvester** are with the Department of Electrical Engineering and Computer Science, University of Michigan, Ann Arbor, MI 48109 USA (e-mail: blaauw@umich.edu; dmcs@umich.edu).

Digital Object Identifier: 10.1109/JPROC.2016.2547946

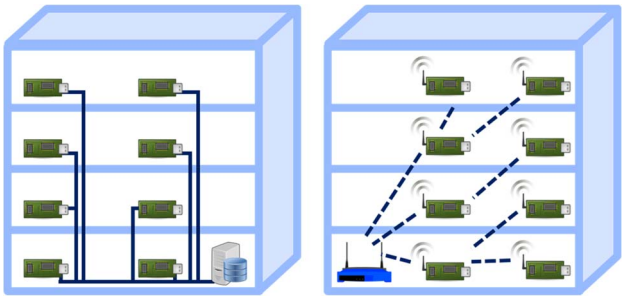

Fig. 1. *Conceptual diagram of the (left) wired sensor node and (right) WSN.*

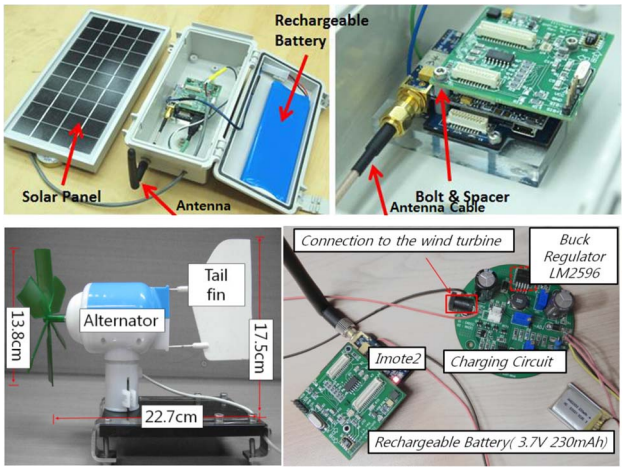

Fig. 2. *WSN with (top) solar energy harvesting [27] and (bottom) wind energy harvesting [29].*

integrity of a bridge, the response to an acoustic emission can be measured from girders [10]. The measured analog data are converted to digital for further data processing using an analog-to-digital converter (ADC). The digital data are then analyzed in the frequency domain to detect a shift in response or resonance frequency. This is the indicator for structural damages such as corrosion, cracking, and physical damage. The abstracted form of data, such as a response magnitude or frequency, significantly reduces the amount of data to be stored in the sensor node or central data repository; it also reduces the amount of data transmission to a higher level system for further analysis on global structural health.

Early SHM systems used wired connections, as shown in Fig. 1, for reliable power delivery and communication among sensor nodes and data repositories [11], [12]. Installation of a wired system was labor-intensive and costly: the system presented in [11] had 12 sensor channels and cost more than $5000 per sensing channel. The cost per wired sensing channel rapidly increases with a larger scale monitoring system. For example, the monitoring system on Bill Emerson Memorial Bridge in Missouri, USA, uses 84 wired sensors accelerometers with an average cost of over $15 000 per channel. More than 600 sensors were installed on Tsing Ma Bridge in Hong Kong, with an average cost per channel of over $27,000 [12].

Wireless sensor nodes (WSNs) initially drew the attention of research communities because they could significantly reduce installation costs by removing wires. Early WSNs developed by SHM research community typically included a few analog-to-digital converter (ADC) channels, a simple 8-b microprocessor with 2–5 MHz of operation frequency, 10 s of kilobyte of memory, and wireless transmitters that could reach hundreds of meters [13]–[15]. These WSNs relied solely on 9- or 1.5-V AA-size commercial batteries without any secondary energy sources such as energy harvesters. Due to the high power consumption of radio communication (e.g., 130 mW for [13] and 900 mW for [15]), radio needed to be duty cycled; the sensor node power budget could be easily dominated by radio power with continuous radio operation.

Energy consumed for radio communication could be reduced by locally processing sensor measurement data and only transmitting useful processed data. Therefore, SHM researchers implemented WSNs with higher processing power. For example, a 32-b processor was introduced with the WSN in [16] and operation frequency as high as 233 MHz was used with a WSN in [17]. To maximize the benefit of high processing power, a heterogeneous dual-core system was proposed in [18]; a low-power 8-b microprocessor was used for overall real-time sensor node operation, and a high-power 32-b microprocessor with a floating-point arithmetic and logic unit was dedicated for intensive data processing. Equipped with a high-energy-density Li/FeS_2 7.5-V battery pack, the dual-core sensor node could achieve an estimated lifetime of one year in the field.

As WSNs become more popular in the SHM researcher community, and as new applications for WSNs in SHM are introduced, WSNs with longer lifetime and in various form factors must meet the unique requirements of new applications. This paper discusses recent trends in WSNs for SHM. Section II reviews how WSNs are evolving to satisfy the needs in new applications. Section III discusses potential circuit design techniques that can be utilized for future ultralow power WSN.

II. RECENT TRENDS IN WSNs FOR SHM

Early WSNs for SHM were typically composed of multiple components on a printed circuit board (PCB), including a microprocessor, sensor interface such as ADC, and a wireless antenna and battery. Batteries were prime cell batteries and could not be recharged with the WSN.

TABLE 1 Harvestable Ambient Energy Sources

Energy Source	Power Density	Source
Acoustic Noise	0.003μW/cm^3 @ 75dB 0.96 μW/cm^3 @ 100dB	[19]
Temperature Variation	10 μW/cm^3	[20]
Ambient RF	1 μW/cm^2	[21]
Ambient Light	100 mW/cm^2 (direct sun) 100 μW/cm^2 (illuminated office)	
Vibration (micro generator)	4 μW/cm^3 (human motion -Hz) 800 μW/cm^3 (machine -kHz)	[22]
Vibration (Piezoelectric)	200 μW/cm^3	[23]
Wind	1 μW/cm^2	[24]
Thermoelectric	60 μW/cm^2	[25]

Fully depleted batteries had to be replaced in the field, which could potentially be very costly when the sensor nodes were installed in hard-to-reach places. This could diminish the cost benefit of WSNs, compared to wired sensor nodes. At the same time, having bulky batteries for longer lifetimes was also unattractive; some applications allowed limited volume for a sensor node's installation. To overcome these challenges, WSNs with energy harvesting became popular to reduce the frequency of battery replacement, or even to achieve energy-autonomous operation. Batteryless form factors were also proposed to achieve tiny sensor platforms; this enables new applications that were impossible with traditional bulky batteries.

A. Energy Harvesting

Energy harvesting is the process of extracting ambient energy from the environment and converting it to electrical energy. Some traditional ambient energy sources, such as solar energy and wind energy, have already been harvested on a large scale with solar power plants and wind turbines because of their abundance and renewability. In the early 2000s, designers began implementing sensor-node-level solar and wind energy harvesting with sensor nodes for civil structure monitoring.

Table 1 summarizes potential ambient energy sources that could be considered for SHM sensor applications. Although there are many different types of available energy sources, practicality of the sources is determined by conversion efficiency of the harvesting modules such as solar cells and thermoelectric generators and environmental conditions at the point of sensor deployment. In recent works, energy harvesting with solar, wind, and vibration energy has been demonstrated for SHM applications.

When monitoring a bridge structure, WSNs must be installed on the bridge frames and wires where they can sense the vibration or tension of the structure. WSNs can also be exposed to the environment in these locations for ambient energy harvesting from surrounding environment. Taking advantage of solar energy harvesting with a bridge monitoring sensor was first proposed in [26], in which a sensor node was used for continuous vibration monitoring. The sensor node only lasted about 5 h with a 9-V battery due to high power consumption and continuous system operation. The sensor nodes were estimated to last more than a year with solar energy harvesting but they would have required a fairly large solar panel and an additional battery to last overnight.

The feasibility of solar energy harvesting with SHM was more fully examined later with WSNs in [27], shown in Fig. 2, installed on the Jindo Bridge in Korea. The sensor node was based on Imote2, a commercial sensor platform developed by Intel [28], which was equipped with a Solarworld SPE-350-6 solar panel (9 V–350 mA) and a 10-Ah lithium–polymer rechargeable battery. The sensor node could monitor bridge vibration and environmental conditions—temperature, wind, light, and humidity—in real time. To minimize the energy consumed for radio communication, wireless data transmission was only activated once a day. The 1.5 months of harvesting operation successfully demonstrated the feasibility of solar energy harvesting; the battery voltage of the solar harvesting sensor node was almost identical to the initial level for 1.5 months, whereas the battery voltage of the sensor nodes without harvesting dropped below the required level (3.6 V) after two months of operation.

Wind is another widely available ambient energy source for SHM, especially for civil structure monitoring. Unlike solar energy harvesting, wind energy harvesting can take advantage of the fact that an ambient energy source (i.e., wind) is readily available day and night, even on cloudy days. The feasibility of wind energy harvesting was also demonstrated with a bridge monitoring application [29], shown in Fig. 2. A small wind turbine generator was estimated to generate enough power for one-cycle operation of an Imote2-based sensor node in 1 h in realistic conditions. In [30], an example wildfire monitoring sensor node with a miniaturized wind turbine generator was demonstrated to generate 7.7 mW of power with low wind speed of 3 m/s with proper voltage conversion and maximum power-point tracking.

For monitoring moving structures or structures that continuously experience vibration, mechanical vibration is another viable source for energy harvesting. Researchers have long been investigating potential of piezoelectric material-based (such as lead zirconate titanate, PZT) energy harvesters. An early example in [31] shows that a PZT-based energy harvester installed in a shoe could harvest 2 mJ per step, which is enough energy for transmitting a 1-b ID more than six times with an active radio-frequency identification (RFID) tag attached to the shoe.

PZT-based energy harvesters are now frequently integrated with WSNs for SHM. For example, a cantilever structure PZT energy harvester for sensing tire deformation was demonstrated in [32]. With four cantilever

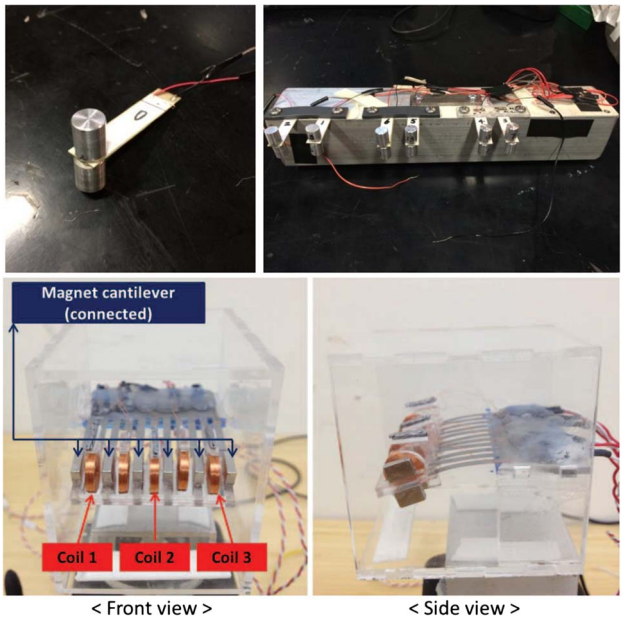

Fig. 3. ***Vibration energy harvesting (top) with cantilevered PZT-based harvester [34] and (bottom) electromagnetic harvester [36].***

harvesters, the sensor node can harvest enough energy (1.2 μJ/rev) for operation, taking 100 data measurements and transmitting 5 B of wireless data. A similar cantilever structure PZT was also used for harvesting 195 μW of power from a 60-Hz vibration of a three-phase alternating current (ac) induction motor [33]. When tuning the natural frequency of the cantilever structure by adjusting the proof mass, 200 μW of power was harvested from railroad vibrations in [34] with the system shown in Fig. 3.

Another well-known method of converting vibration energy into electrical energy is using an electromagnetic generator. An electromagnetic generator consists of a permanent magnet and a coil. When the magnet vibrates due to vibrations of the attached structure, an electrical current is induced on the coil. Many researchers have implemented WSNs for SHM with such electromagnetic generators. For example, a 3.15-cm^3 miniature electromagnetic generator was built with four magnets and a cantilevered coil [35]. The electromagnetic generator was mounted on the engine block of a car, which generated an average of 157 μW of power. Both the magnets and coils were cantilevered in [36] to maximize power harvesting from low frequency ($\sim$3 Hz) bridge vibrations. When a 15-ton dump truck drove over the bridge, the electromagnetic harvester could harvest up to 30 μW of power from the vibrations.

Rather than continuously harvesting from ambient energy, another option for sensor node operation is to deliver energy to a sensor node periodically, i.e., when a

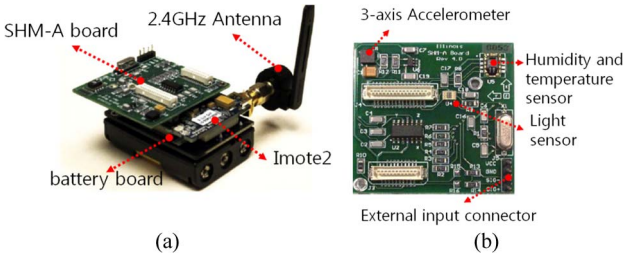

Fig. 4. ***WSNs based on the commercial sensor platform Imote2 [41]. (a) Imote2. (b) SHM-A board.***

measurement is taken. This enables batteryless operation of WSNs, which is similar to a passive RFID. For example, the highway bridge monitoring sensor in [37] was equipped with a contactless power delivery system; it successfully delivered 67.5 mW of power to the sensor and wireless transmitter. However, the contactless power delivery distance was limited since it was using near-field magnetic coupling for power delivery. Longer range power delivery was demonstrated with a mobile agent in [38]. Using a 5.8-GHz grid antenna for power transmission and a patch antenna array for power reception, a mobile-host RC vehicle could deliver $\sim$120 mW of power to bridge girder monitoring sensors at up to 60 cm.

With advances in low-power electronics, exploiting galvanic corrosion as a form of energy harvesting was proposed for WSNs for marine SHM [39]. Using carbon and magnesium electrodes, the galvanic harvester could generate peak power of up to 4.7 mW at the output.

B. Platform Size Reduction

Early WSNs for SHM required bulky batteries, such as a commercial 9-V battery, to provide enough lifetime for power-hungry sensor node operation without energy harvesting. Therefore, overall system volume was on the order of thousands of cubic centimeters. With advances in low-power electronics and utilization of energy harvesting, the size of today's WSNs for SHM could be reduced with smaller batteries. Moreover, growing demand on SHM research resulted in standardized commercial WSN platforms such as IMote series [28] and MICA [40] motes. These sensor platforms operate with 1.5-V AA or AAA size alkaline batteries; hence the volume could be reduced to tens of cubic centimeters. They also provide a proven platform for SHM researchers, which enables quick implementation of custom sensor nodes by adding custom features of interest to the skeletal sensor platform as shown in [41] as shown in Fig. 4. Therefore, these commercial sensors are frequently used for SHM research in a wide range of applications.

Despite the advances in low-power electronics and battery technologies, a sensor node's lifetime is still limited to months and years. Although energy harvesting has the

potential to significantly extend the lifetime of WSNs, there are still many applications in which no ambient energy is accessible. Moreover, some applications require a small sensor node volume for installation in limited space. One attractive solution for these issues is building WSNs based on RFID technology. For RFID-based sensor nodes, power is delivered with an interrogator through near-field inductive coupling whenever sensor operation or identification is required. With the collected power, the sensor node takes measurements and transmits data to the interrogator. This scheme enables indefinite sensor node operation as long as the sensor node hardware remains functional. It also allows batteryless sensor node operation where sensor node volume can be significantly reduced with the removal of a battery.

Sensor nodes for sensing corrosion [42], [43], and cracks [44] of steel beams in concrete and concrete curing conditions [45] are good examples of taking advantage of an RFID-based system. These sensor nodes are embedded in concrete blocks; hence, the small volume minimizes the impact on structural integrity. Since the sensor nodes are surrounded by firm concrete, there are not many ambient sources of energy to be harvested such as light and wind. Moreover, to monitor structural integrity of steel and concrete, sensor node lifetime should be similar to the structure itself. RFID-based sensors are now employed for a wide range of SHM applications, including strain sensing [46], ultrasound monitoring [47], and more.

Recently, sensor nodes based on custom-designed integrated circuits (IC) were introduced. Custom-designed IC-based sensor nodes can operate at ultralow power—as low as the submicrowatt order. This is possible because all unnecessary features in over-the-counter product IC can be removed and the circuit implementation can be optimized for the application needs of a custom-designed IC. For example, an IC designed for a sensor node in [48] only consisted of a rectifier, current reference, and floating gate array for storage; these are the minimum features required for sensing, data processing, and data storage. Although this prototype did not include an RF interface, it demonstrated that sensing, data processing, and data storage can be accomplished with a 1 μW power budget with a custom-designed IC.

With ultralow power consumption of a custom-designed IC, the sensor system in [49] demonstrated the concept of "self-powered operation"; this means that power for continuous structural health and usage monitoring is scavenged from ambient energy sources. The sensor system is based on the custom-designed IC shown in Fig. 5. The IC uses seven floating gate injectors that consume 800 nW for computing and storing the strain level-crossing statistics [50]. The power required for continuous monitoring can be supplied by a 1 cm^3 piezoelectric transducer (PZT-5H) at strain levels of 100 $\mu\epsilon$ and at a frequency of 1 Hz, achieving self-powered operation.

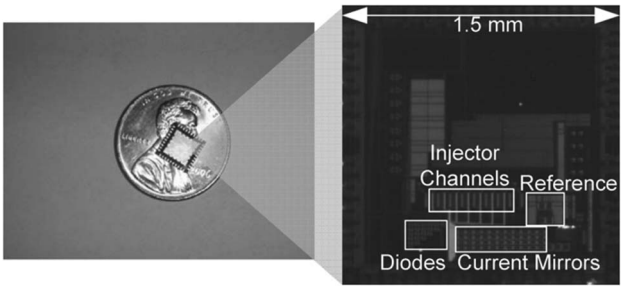

Fig. 5. ***Custom-designed IC for WSN [50].***

For data retrieval, an RFID-like passive power delivery is used to provide 90 μW of power for A/D conversion and data transmission by carrier backscattering.

Recent advances in ultralow power IC design enabled a miniature sensor node in the mm^3-scale volume [51]. The mm^3-scale sensor node created exciting new opportunities for SHM by significantly reducing the sensor system volume to the order of a single-digit cubic millimeter, and reducing active power ($\sim$50 μW) and standby power ($<$ 10 nW). The mm^3-scale sensor platform consisted of layers of custom-designed sensor nodes (Fig. 6). Each layer includes a few dedicated function units such as a microprocessor, memory, an imager, and a timer. One of the layers is a thin-film Li battery whose energy density is only 1 $\mu Ah/mm^2$ [52]. To operate the sensor node given such a stringent energy budget, each functional unit must be carefully designed with extremely low power and on-time budget.

The sensor node was also demonstrated with a nanowatt-level energy harvester that could harvest 3 nW from dim indoor light [53]. This opens up the possibility of operating a sensor node with energy harvested from sources that have not been traditionally considered, such as those with nanowatt output power or of extremely small size. A few sensing modalities that can be useful for SHM are also demonstrated with a power and energy budget of a mm^3-scale sensor platform, as shown in Fig. 7. Pressure sensing was demonstrated in [54] with a dual-slope capacitance-to-digital converter, where pressure could be measured in 0.77-mmHg resolution with 110 nW of power consumption. Temperature sensing with 0.3 °C resolution was demonstrated in [55] with consuming 2.2 nJ of energy per conversion and 70 nW of power. Imaging with 160 $\times$ 160 pixels or motion detection with 10 $\times$ 10 pixels was demonstrated with 304 nW of power consumption in [56].

There are still limits on the types of available sensing modalities and other supporting functions that can be implemented with a power and energy budget of mm^3-scale sensor platforms. However, the recent surge of low-power electronics research is enabling a wider range of SHM applications, especially with low-power

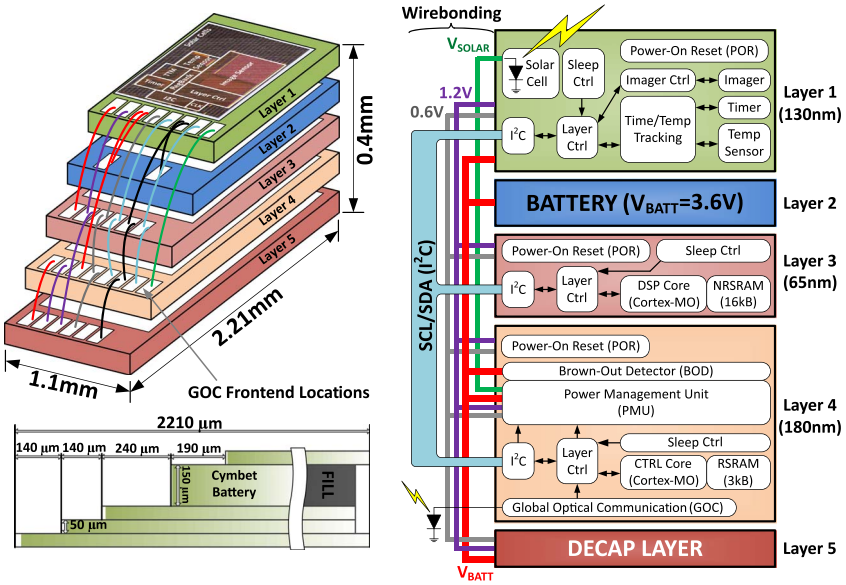

Fig. 6. *Layer structure and block diagram of custom-designed IC-based sensor nodes in mm³ volume [51].*

WSNs with custom-designed ICs. In the next section, a promising state-of-the-art low-power circuit design technology will be introduced for a range of functions. By reducing the active power below the submicrowatt order, these advanced low-power circuits are expected to significantly expand the lifetime of not only the WSNs based on a mm^3 platform but also generic custom IC-based WSNs.

III. ULTRALOW POWER CIRCUIT DESIGN FOR WSNs FOR SHM

The typical sensor node system consists of many, or all, of following function blocks: microprocessor, memory, power management unit, energy harvester, wakeup timer, sensor interface, radio transmitter and receiver, among others. There are a wide range of design options for each of these functional blocks since there are power-performance or volume-performance tradeoffs among available options. For example, for a power management unit, an off-chip inductor-based buck/boost direct current to direct current (dc–dc) converter topology will be preferred when finely tunable voltage conversion ratio is required with large loads (on the order of milliwatts). On the other hand, on-chip switched capacitor (SC)-based dc–dc converter will be preferred if volume minimization is critical. However, due to structural limitations of SC-based converters, voltage conversion with only a few fixed conversion ratios with small loads (submilliwatt) is applicable. Moreover, within SC-based converter design options, there are a wide array of converter topology options, which determine the conversion ratio, and operation frequency, which is directly related to the converter load range.

Although there cannot be universal guidelines for selecting design options on hardware implementation of SHM sensors, the following criteria should be carefully considered for design option selection for hardware implementation.

1) System Volume Constraint

System volume plays a role in two ways. First, battery volume often occupies a significant portion of system volume in small sensor node systems. This battery volume determines the amount of energy the system can utilize before the next charging event. Therefore, with recharging cycle time, which is determined by usage model, average system power can be determined. Each functional block should be carefully designed to remain within this power budget.

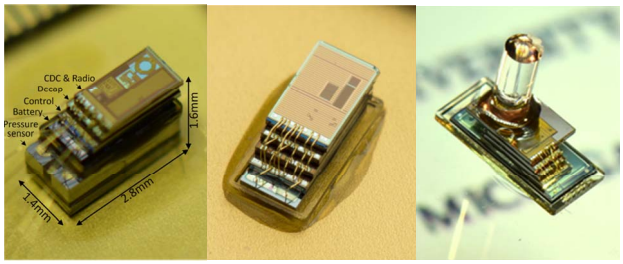

Fig. 7. *Example (a) pressure, (b) temperature, and (c) image/motion detection sensor in mm³ sensor platform [54]–[56].*

Second, certain applications can place stringent volume limits on a system, for example, whether the sensor should be deployed in a limited space or embedded in the structure itself (i.e., in a concrete wall). In this case, design options that minimize the use of off-chip components (inductors, capacitors, off-chip antenna, crystal oscillators, etc.) should be selected.

2) Usage Model

A sensor node system usage model often determines the implementation option for many functional blocks. For example, the charging model—how often the system battery should be recharged, or how much energy can be harvested from the ambient environment—largely determines the battery size, necessary duty cycles, and other parameters. Another example is the communication model; large differences exist between nodes communicating with a base station with wired power and those communicating to an adjacent sensor node with limited power budgets. For base station communication, no accurate timer for synchronization is required on-node since the base station is always listening. On the other hand, an accurate timer is required for accurate node-to-node communication synchronization to minimize receiver activation power.

Generally, reducing power consumption of individual functional blocks provides a better tradeoff space for the larger system, in terms of power versus performance or size. In this way, ultralow power implementation of certain units can totally change the usage model of the entire system: significant power reduction of a power-dominant function can dramatically improve duty cycle, opening up new applications. Therefore, block-level low power design is a key part of achieving ultralow power sensing systems. Recent innovations in low-power circuit design research are enabling sensor node systems to operate at unprecedented low power levels. For example, Figs. 8 and 9 show the state of the art for ADCs and low-power static random access memories (SRAMs). ADC energy per conversion step is a common metric for data converter energy efficiency and has seen steady and rapid progress over the past two decades [57]. Fig. 9 highlights the tradeoff between memory density (measured by the size of an individual bitcell relative to technology feature size F) and standby power, which is a critical metric for sensor node design. In this section, we present several ultralow power circuit designs that are key components of WSNs for SHM.

A. Low-Power Energy Harvesters

Harvesting energy with high efficiency has always been a high-priority challenge for energy harvesters. However, harvesting energy efficiently at a low power level is a new challenge for sensor nodes that harvest energy from ambient sources. For example, an energy harvester in [50] harvested less than 1 μW from ambient vibrations with a 1-cm^3 piezoelectric transducer for its long-term operation. Maintaining reasonable efficiency below a microwatt is a tricky challenge, since power consumed for an operating harvester could easily exceed a microwatt. Recently, two circuit design techniques were proposed to enable efficient energy harvesting at a power level as low as a single-digit nanowatt, from very weak ambient sources such as indoor light [58] and endocochlear biopotential [59].

The energy harvester in [58] was based on SCs that could be fully integrated on-chip. A typical SC-based energy harvester consists of three parts: a clock generator, a level shifter, and a switched capacitor network (SCN). The efficiency of an SC-based harvester is typically limited by the overheads for clock generation and level

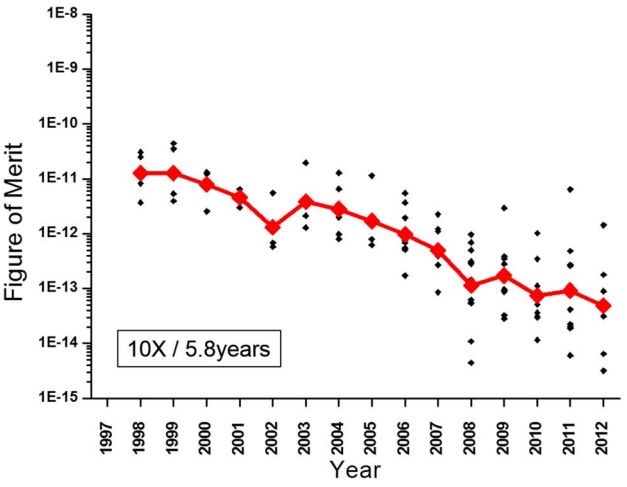

Fig. 8. *Efficiency improvement of ADCs (figure of merit = J/conversion step) [57].*

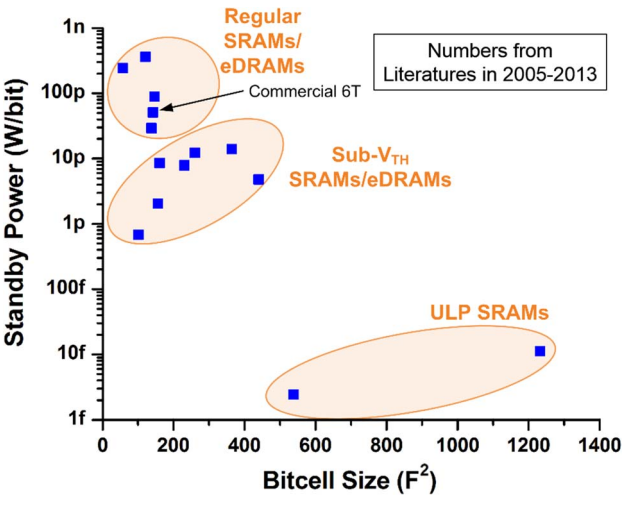

Fig. 9. *Power versus bitcell area tradeoff for static memory.*

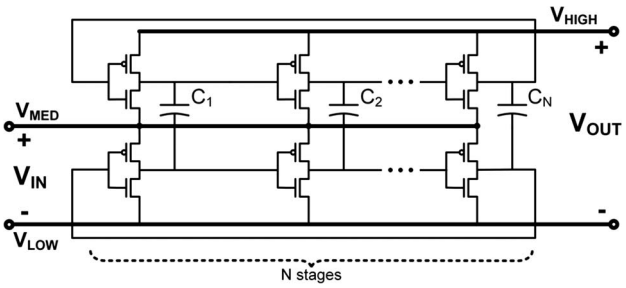

Fig. 10. ***Efficient self-oscillating voltage doubler which internalizes clock generation and level conversion [58].***

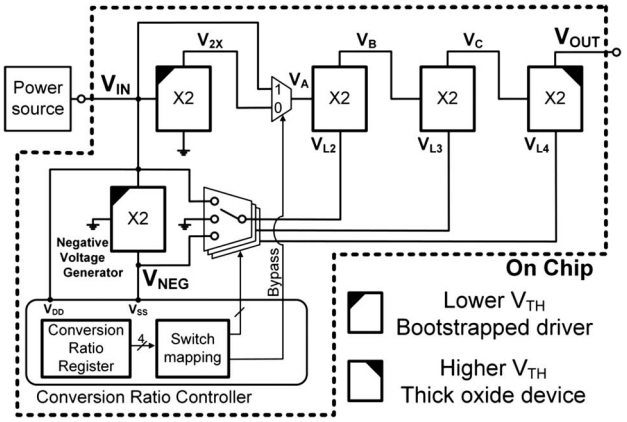

Fig. 11. ***Overall structure of the energy harvester based on the self-oscillating voltage doubler [58].***

conversion to driving switches in an SCN. Hence, no SC-based energy harvester has been demonstrated below the microwatt range. The SC-based energy harvester in [58] was built with a cascaded self-oscillating voltage doubler that internalized oscillation and reduced clock power and level conversion power overhead.

Fig. 10 shows the structure of self-oscillating voltage doubler where two ring oscillators are stacked. Each stage of the ring oscillator is coupled by flying capacitors $(C_1, C_2, \ldots, C_N)$. Assuming V_{LOW} is connected to the ground and V_{MID} is connected to the harvesting source, as inverters in the top and bottom rings charge or discharge the flying capacitors, charges are transferred from the middle rail (V_{MID}) to the output rail (V_{HIGH}). The transition in one stage also triggers a transition in the next stage, performing a multiphase dc–dc conversion with an overlapping charge/discharge phase. Therefore, the stacked ring oscillator eliminates the need for an additional clock generator and level converters, which significantly reduces overhead. In addition, the oscillation self-starts with a harvester output of > 140 mV, allowing self-powerup of the sensor node with a completely depleted battery.

The overall energy harvester architecture is shown in Fig. 11. One voltage doubler is used to generate a negative voltage (V_{NEG}) by connecting the mid rail to ground and the high rail to the harvester input. By cascading the voltage doublers and selectively connecting the low rail of each doubler stage to a harvester source, ground, or generated negative voltage, the overall conversion ratio can be controlled from $9\times$ to $23\times$. With a wide conversion ratio range, energy can be harvested at a range from 5 nW to 5 μW with a reasonable efficiency of $> 40\%$.

Another nanowatt-level energy harvester based on an inductive boost converter was demonstrated in [59] as shown in Fig. 12. Several circuit design techniques for ultralow power operation were used for the energy harvester to achieve high efficiency at a nanowatt power level. This was accomplished by minimizing efficiency loss due to switching the overhead and leakage current. Using the on-chip inductor for the boost converter requires a high switching frequency since the on-chip inductor typically has a small inductance on the order of nano-Henry (nH). Therefore, a 47-μH off-chip inductor was used to lower the switching frequency of the boost converter to as low as 12.8 Hz; this significantly reduces the switching overhead for the two transistors $(N0, P0)$ in the boost converter.

To reduce leakage, a picowatt charge pump circuit was used to minimize the leakage in the boost converter. Instead of turning off the PMOS $(P0)$ connecting the inductor to the load with the regular supply voltage (V_{DD}), the doubled voltage (V_{PUMP}) generated by the charge pump was used to suppress leakage through $P0$ by applying a negative V_{gs} (i.e., super cutoff). Furthermore, ultralow power control circuits were implemented to tune the circuits for input impedance and zero current; this achieved quiescent power consumption of 544 pW. With energy harvesting the source modeled by a Thevenin voltage of 100 mV and a Thevenin resistance of 1 M Ω, the harvester could harvest up to 1.4 nW and achieve a maximum conversion efficiency of 56%.

B. Low Power Timers

Timers in WSNs play a critical role of determining when the sensor measurement should be taken and when the wireless data communication should be performed. Therefore, an accurate timer, especially in terms of long-term jitter [60], is necessary for minimizing the error in the measurement interval. Moreover, a timing error for radio transmission can be very expensive in terms of energy. For node-to-node communication, if there is a timing error between timers in communicating nodes, one node should turn on its receiver and wait for the other node to respond. This is a very costly operation since the typical radio receiver consumes at least hundreds of microwatts of power. Since the high accuracy timers typically have higher power consumption, there

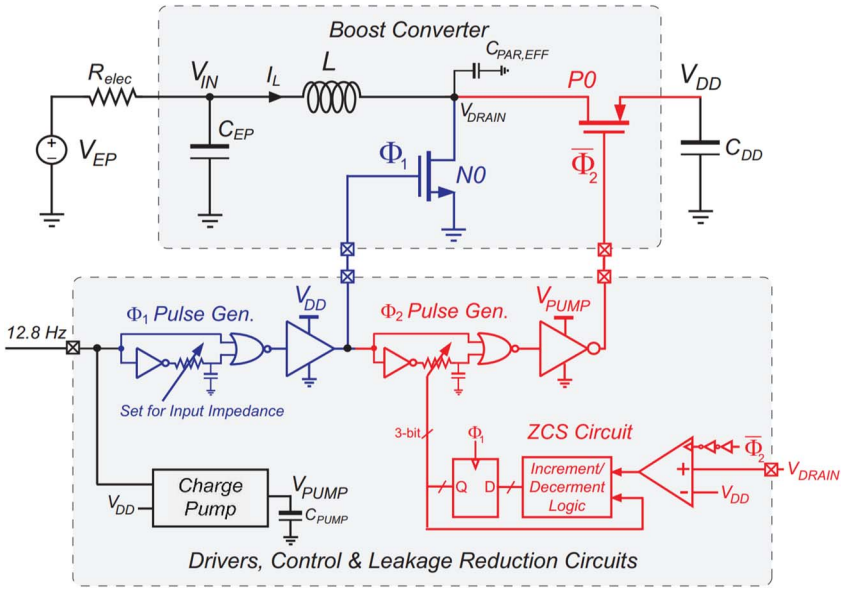

Fig. 12. ***Overall structure of a boost-converter-based nanowatt energy harvester [59].***

exists a tradeoff between power consumption on timer and radio receiver. Therefore, the WSN designer should carefully choose the type of timers that meets both accuracy requirement and power budget of the WSN. If there is an always-on receiver (i.e., the base station), which is often continuously powered with wired power connection, accuracy requirement can be relieved and less accurate low power timer could be used for target WSN. Despite the importance of timer accuracy, an allocable power budget for timers in low power WSNs is limited since the timer is a component that cannot be duty cycled and should stay on continually. Hence,

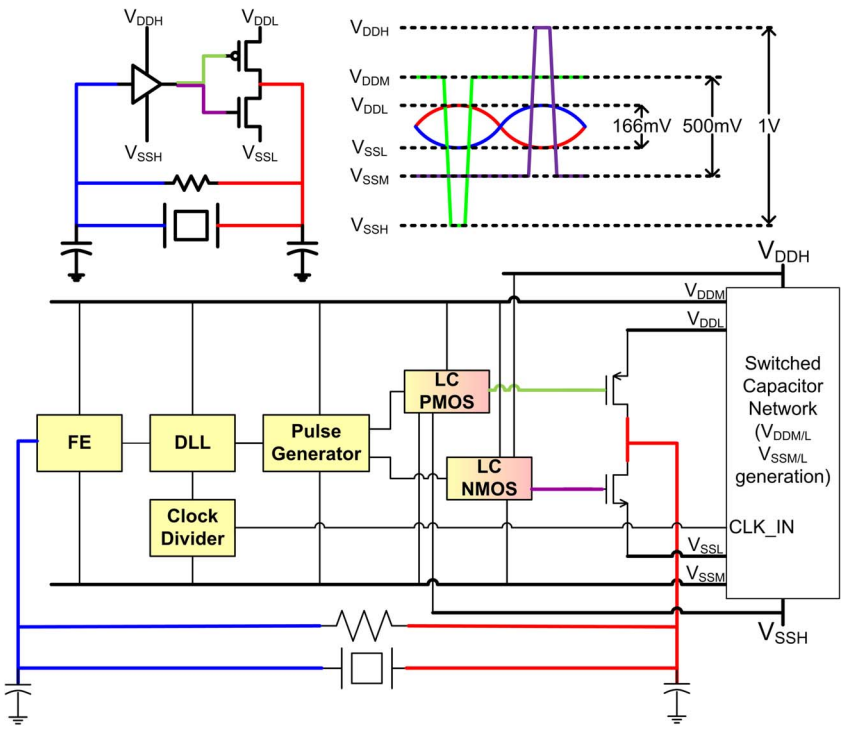

Fig. 13. ***Overall structure of the DLL-assisted crystal oscillator in [65].***

designing a low power timer with acceptable accuracy has been one of the key challenges for developing ultralow power WSNs.

Quartz crystal has been a traditional source of accurate timing, with a power consumption typically on the order of a microwatt or hundreds of nanowatts: 220 nW for 32.768 kHz [61] and 700 nW for 2.1 MHz [62]. Microelectromechanical systems (MEMS)-based oscillators [63], [64] could be an option for volume-limited applications since they achieve comparable accuracy without bulky crystals. But their power consumption is on the hundreds of nanowatts level; this could be acceptable for some sensor nodes but not for ultralow power sensor nodes such as the one shown in [48], whose power budget for the entire system was only 1 μW.

Recently, a delay-locked loop (DLL)-assisted crystal oscillator (XO) was introduced with a power consumption as low as single-digit nanowatts and an acceptable accuracy for periodically synchronizing WSNs [65]. Earlier low power XOs focused on oscillation amplitude reduction, which reduced power consumption by minimizing energy lost per cycle. This could make an XO unstable since excess amplitude reduction means the input voltage to the oscillator driver could be as low as below-threshold voltage of driver transistors. The proposed DLL-assisted XO utilized an amplifier stage to mitigate the weak driver issue and three power domains to achieve low power consumption. The overall structure is shown in Fig. 13. The front-end (FE in Fig. 13) amplifies the oscillation swing from the low voltage domain (V_{DDL}/V_{SSL}) to the medium domain (V_{DDM}/V_{SSM}). The amplified oscillation is fed to the DLL, which triggers the pulse generator under the high voltage domain (V_{DDH}/V_{SSH}) to driving NMOS/PMOS. Note that the gate of driving PMOS/NMOS is driven at a high voltage domain through the level converters (LC PMOS and LC NMOS in Fig. 13) for stable operation, but the source of driving transistors is connected to the low domain for the reduced oscillation swing. The DLL-assisted XO consumed 5.58 nW of power for 32.768-kHz oscillation with XO-comparable accuracy (supply sensitivity of 17.6 ppm/V and temperature sensitivity of 1.32 ppm/°C)

A complementary metal–oxide–semiconductor (CMOS)-based on-chip timer with a constant charge subtraction scheme [66] was also introduced to achieve 5.8 nW of power consumption with a slightly worse temperature sensitivity (Fig. 14). The volume and manufacturing cost of the WSN could be reduced with the on-chip timer, as opposed to a crystal-based timer. In conventional relaxation oscillators, a period is measured by detecting when the voltage at the load capacitor reaches a threshold. Therefore, a period in the relaxation oscillator can be represented as the total time it takes to charge a load capacitor and the time delay of the threshold detection circuit (i.e., comparator). The charging time could be made temperature insensitive by carefully

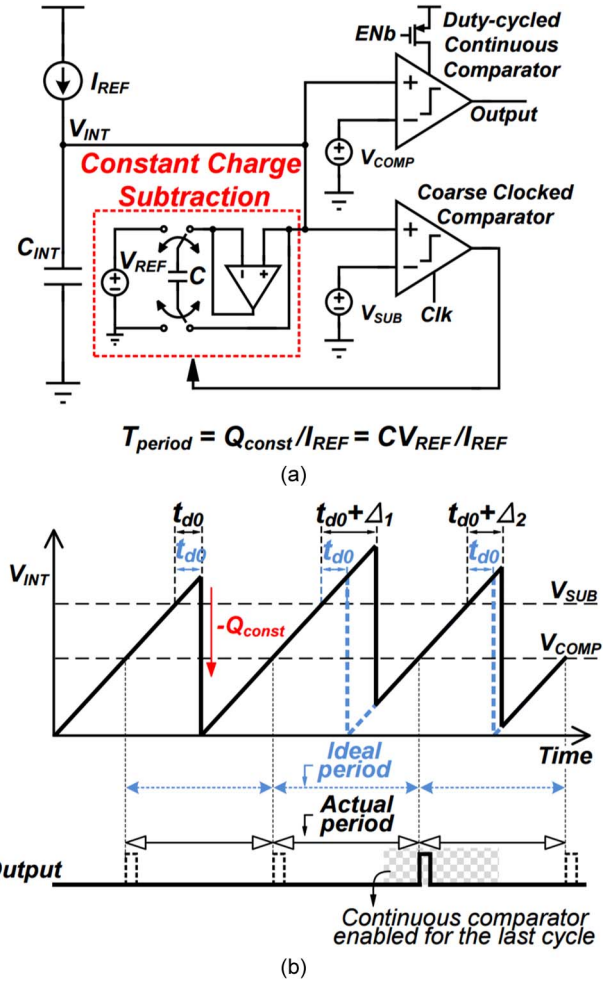

Fig. 14. *(a) Overall structure and (b) timing diagram of the on-chip CMOS timer with a constant charge subtraction scheme [66].*

designing a temperature-insensitive current source. However, the threshold detection was performed by a comparator whose delay was a typically strong function of the temperature. The proposed on-chip timer used a constant charge subtraction scheme [Fig. 14(a)] to eliminate the detection delay from the timer period. Instead of fully discharging the load capacitor each period, the constant charge was subtracted from the load capacitor when the voltage reached the threshold for subtraction (V_{SUB}). Meanwhile, the voltage comparison for the period measurement was performed at a different level (V_{COMP}). This guaranteed that the period measurement was accurately taken, even if the charge subtraction was performed with a time variation, as shown in Fig. 14(b). To minimize power consumption, a clocked comparator was used to detect the charge subtraction threshold and a duty-cycled comparator was used for the period measurement. The on-chip timer consumed 5.8 nW for 11-Hz oscillation. Temperature sensitivity of the timer was 45 ppm/°C.

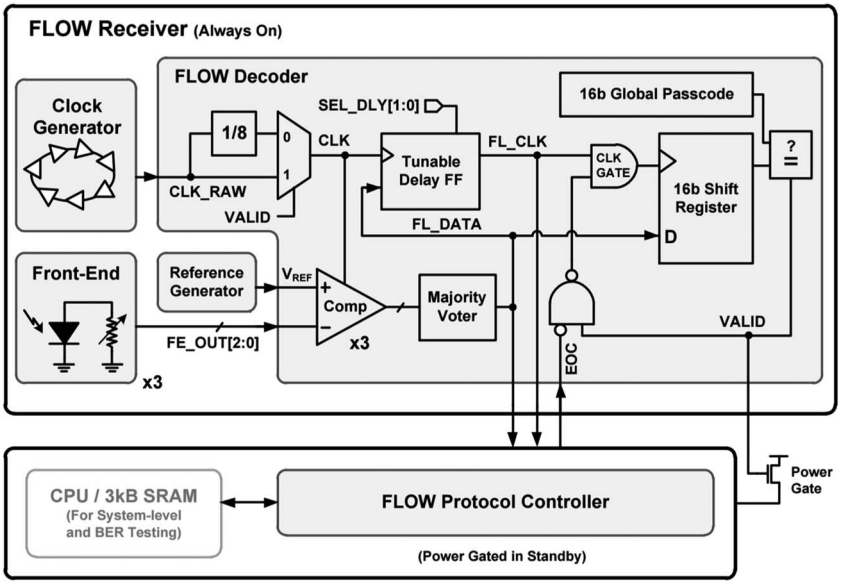

Fig. 15. ***System block diagram of FLOW [71].***

C. Low Power Wakeup Receivers

Low power WSNs are often heavily duty cycled to minimize active power consumption. Therefore, most of the electronics stay in the standby mode for most of the time. However, a sensor node must interface to the user to allow the user to interrupt, synchronize, and reprogram the sensor node at any time. Hence, the wakeup receiver is an essential element in WSNs. Since wakeup receivers should be always on, even in the standby mode, to be ready for user interaction, minimizing power consumption is critical.

Conventional implementation of a wakeup receiver is with a low-sensitivity RF receiver. Due to high carrier frequency and throughput, RF solutions typically consume several tens of microwatts of power, as shown in [67] (75 μW) and [68] (52 μW). Recently, a dual-mode wakeup receiver [69] was introduced that used two modes for operation: 1) low data rate wakeup mode and 2) high data rate reception mode. The receiver stayed in low-data rate and low power wakeup mode most of the time and switched to high power data mode only when a wakeup request was detected. With this duty-cycling scheme, power consumption of the wakeup receiver was significantly reduced to 8.5 μW. An ultrasound-based wakeup receiver was also introduced to take advantage of the low carrier frequency and to sacrifice the data rate for communication [70]. The ultrasound-based wakeup receiver consumed 4.4 μW of power at 250 b/s data rate at 8.6 m, which is acceptable for many structural or environmental monitoring applications. However, power consumption of the microwatt order could still be very expensive for sensor nodes with microwatt [48] or even nanowatt [51] power budgets. At the same time, the cost and volume of an ultrasonic transducer or RF antenna could be an issue for some volume-limited applications.

A wakeup receiver called the Free Low power Optical Wakeup (FLOW) receiver [71] used visible light as an information carrier. By exploiting photosensitivity of diodes on silicon, standby power consumption could be reduced by more than three orders of magnitude compared to the RF and ultrasound wakeup radios. Fig. 15 shows the system block diagram, and Fig. 16 shows the circuit implementation details of the FLOW. In each front-end (FE) unit, an $n+/pw/nw$ parasitic diode is used as a photovoltaic to develop voltage at the anode of the diode when light was shined. When light was not shined, tunable pull down resisters discharged the anode. The voltage at the FE output (i.e., anode of the photovoltaic) was periodically compared to a reference voltage using a clocked comparator. Three sets of FEs and comparators were used so that comparison results could be majority-voted for robustness. In the standby mode, the clocked comparator was operated at low frequency to minimize the standby power of the wakeup receiver to 695 pW. Once a user-defined pattern was detected at low frequency, the operation switched to the high-frequency mode where a higher data rate could be achieved. In high data rate mode, the FLOW consumed 12.7 nW of power at 91 b/s, resulting in 140-pJ/b efficiency. Maximum applicable range with laser light source was 50 m. To minimize static power consumption through leakage, high threshold input/output (I/O) transistors were extensively used for circuit implementation, as shown in Fig. 16.

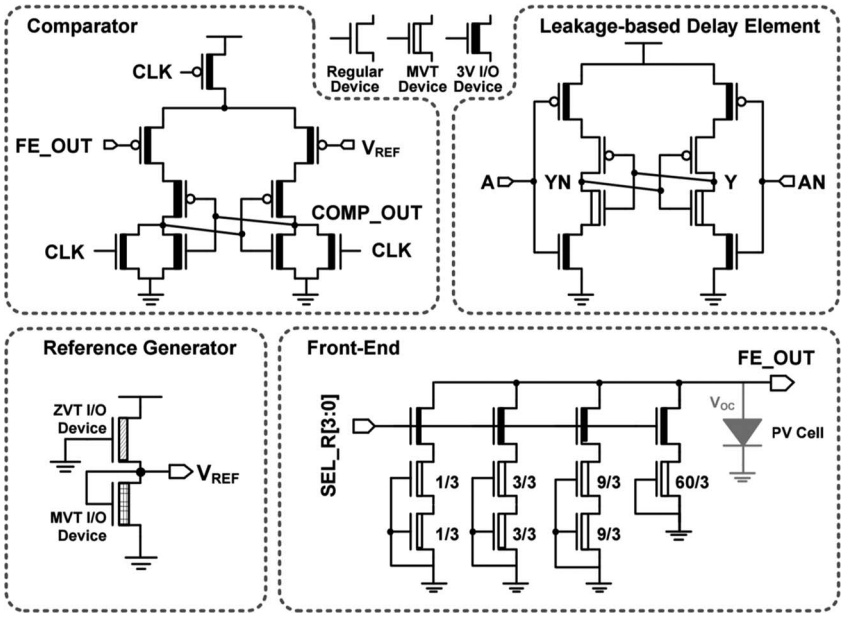

Fig. 16. *Circuit implementation of building blocks in FLOW.*

D. Low Power Sensing Modalities

WSNs require various sensing modalities for SHM applications. However, if power consumption of the sensing modality is too high for the power budget of the entire sensor node system, the sensor must be duty cycled; or comparable power should be harvested to achieve a reasonable lifetime. As ultralow power circuit design techniques have advanced, sensing modalities with submicrowatt power consumption have been developed. Such low-power consumption means that continuous sensing could be accomplished even with ambient energy harvesting; 1 μW of power was harvested in [48].

Temperature sensing is one of the key sensing modalities for SHM. By tracking temperature changes in a single spot (temporal temperature monitoring), thermal variation, which is a good indicator of stress due to thermal expansion/reduction of a structure, can be monitored. Rapid temperature changes also can be indicators for abnormality, such as air or gas leakage, of monitored structure. On the other hand, by monitoring the temperature of multiple spots (spatial temperature monitoring), spatial abnormality, such as HVAC failure in a building, can be detected for structures.

An on-chip temperature sensor typically measures temperature by quantifying the difference between a temperature-dependent and a temperature-independent voltage/current source. Bipolar junction transistor (BJT)-based temperature sensors [72], [73] are the most conventional on-chip temperature sensors. These approaches leverage the fact that base-emitter voltage (V_{BE}) is complementary to absolute temperature (CTAT) and the difference between emitter voltages (ΔV_{BE}) is proportional to absolute temperature (PTAT). However, these temperature sensors showed microwatt order power consumption since a power-hungry ADC was used to digitize voltages. A fully integrated CMOS temperature sensor in [74] was developed that consumed less than 100 nW of power. The CMOS temperature sensor introduced a novel MOSFET-based sensing element to implement a PTAT voltage source with very low power and small area. It also used current-to-frequency and frequency-to-digital conversion schemes to avoid digitization with the power-hungry ADC.

The PTAT sensing element is shown in Fig. 17. The drain current of M_1 and M_2 can be represented with the following subthreshold current equation with the assumption

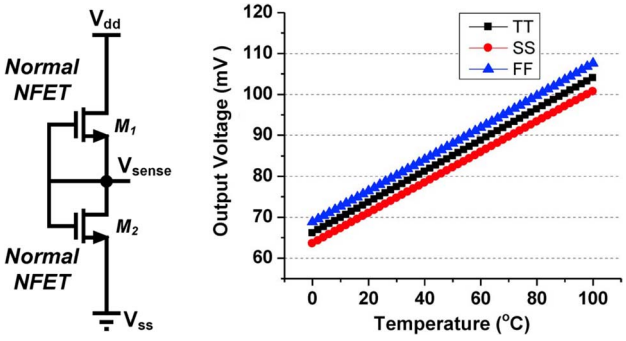

Fig. 17. *Structure of the temperature sensing element in [74] and its simulated temperature response.*

of a long channel device to ignore DIBL and $V_{\text{sense}} > 3V_T$ to ignore dependence to V_{ds}:

$$I_1 = \mu_1 C_{\text{ox1}} \left(\frac{W_1}{L_1}\right) V_T^2 e^{1.8} e^{\frac{-\Delta V_{\text{th1}}}{\eta V_T}} e^{\frac{\left(0 - V_{\text{th1}} - \gamma_1' V_{\text{sense}}\right)}{m_1 V_T}}$$

$$I_2 = \mu_2 C_{\text{ox2}} \left(\frac{W_2}{L_2}\right) V_T^2 e^{1.8} e^{\frac{-\Delta V_{\text{th2}}}{\eta V_T}} e^{\frac{\left(V_{\text{sense}} - V_{\text{th2}} - \gamma_2' 0\right)}{m_2 V_T}}$$

where μ is mobility, V_{th} is threshold voltage, γ' is linearized body coefficient, η is the DIBL coefficient, and ΔV_{th} is the term representing the transistor-to-transistor leakage variations. Equating two current equations yields

$$V_{\text{sense}} = \frac{m_1 m_2}{m_1 + \gamma_1' m_2} V_T \ln\left(\frac{\mu_1 C_{\text{ox1}} W_1 L_2}{\mu_2 C_{\text{ox2}} W_2 L_1}\right)$$

where output voltage V_{sense} is a good linear function of thermal voltage V_T. The PTAT voltage was converted to the PTAT current with the area-efficient conversion scheme shown in Fig. 18. Since PTAT voltage was lower than 100 mV for most of the range, a small resistance could be used for current conversion in nA. This current was mirrored through two transistors (M_P and M_N) to create a current-controlled oscillation. The current-controlled oscillation frequency was compared to a reference frequency to measure the temperature. The CMOS temperature sensor achieved the worst case inaccuracy of +1.5 °C/−1.4 °C; this is acceptable for many SHM applications with 71 nW of power consumption, which allows continuous monitoring for systems with microwatt power budget such as [48].

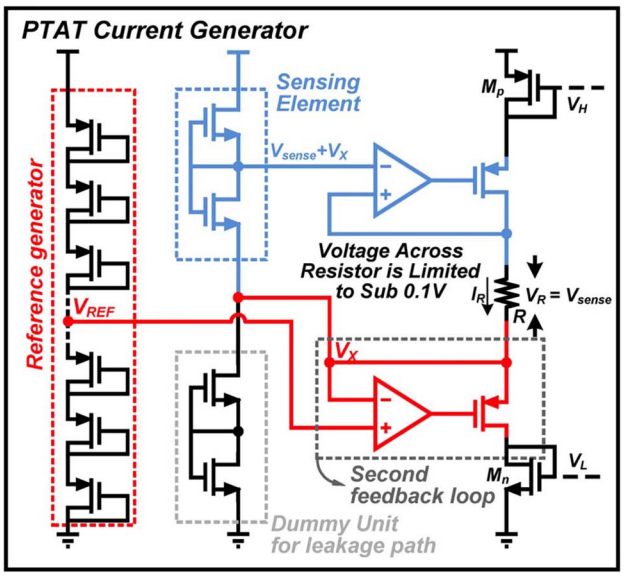

Fig. 18. *Voltage-to-current conversion scheme of the CMOS temperature sensor in [74].*

Capacitive sensing is another key sensing modality for SHM applications. Capacitive sensing can be adopted for a wide range of physical sensing applications, such as pressure [75], displacement [76], and humidity [77]. Pressure changes between girders and supporting steel beam of a building or tension changes on cables of a hanging bridge indicate changes in supported weight of each beam/cable, which could be critical information for early detection of failures. Cumulative humidity monitoring can also help corrosion extent estimation for exposed structures and corrosion detection for enclosed structures.

The capacitance-to-digital converter (CDC) is the key circuit element that digitizes the capacitance value for capacitive sensing. Earlier CDC design research focused on achieving a high resolution. For example, an SC $\Delta\Sigma$ converter [76] achieved a high resolution of 0.065 fF at the cost of high power (14.9 mW). The $\Delta\Sigma$ converter topology required repeatedly charging and discharging the sensor cap in pico-Farad (pF) order, resulting in an inefficient conversion with a figure of merit (FoM = power $\times$ time/2^{ENOB}) of 7380 fJ per conversion step. An alternative topology for CDC is successive approximation (SAR) [78], but it requires a direct connection of sensor capacitor-to-capacitor DAC in SAR ADC. This significantly reduces the voltage swing at the DAC output due to the large capacitance of the sensing capacitor. Since the comparator has limited resolution, this results in a low ENOB of 6.83 b and a high FoM of 7937 fJ per conversion step.

A new CDC that combines the correlated double-sampling approach and the differential asynchronous SAR ADC [79] was proposed to achieve high-conversion efficiency with very low power (Fig. 19). In the first "precharge 1" stage, a reference capacitor (C_{REF}) and a sensing capacitor (C_{SENS}) were series-connected between ground and V_{DD}. The center node was set to virtual ground (V_{REF} or $V_{\text{DD}}/2$). As it switched to the second "sample 1" stage, V_{DD} and ground connections to series-connected $C_{\text{REF}}/C_{\text{SENS}}$ were reversed, charging C_{SPL1} with a charge proportional to $C_{\text{SENS}} - C_{\text{REF}}$. These operations can be repeated with a reversed V_{DD}/ground connection, as shown in "precharge 2" and "sample 2" stages where a second sampling cap C_{SPL2} will accumulate the charge proportional to $C_{\text{REF}} - C_{\text{SENS}}$. Therefore, the two sampled voltages were equal with opposite polarity, which doubled the signal magnitude. At the same time, the offset at the input (V_{OS}) and variations on V_{REF} were all canceled. The sampled voltages were converted to digital values with asynchronous ADC. Since small sampling capacitors (C_{SPL1} and C_{SPL2}) were used for ADC, the large sensing cap (C_{SENS}) was isolated from CDAC, minimizing the degradation of accuracy. The CDC achieved

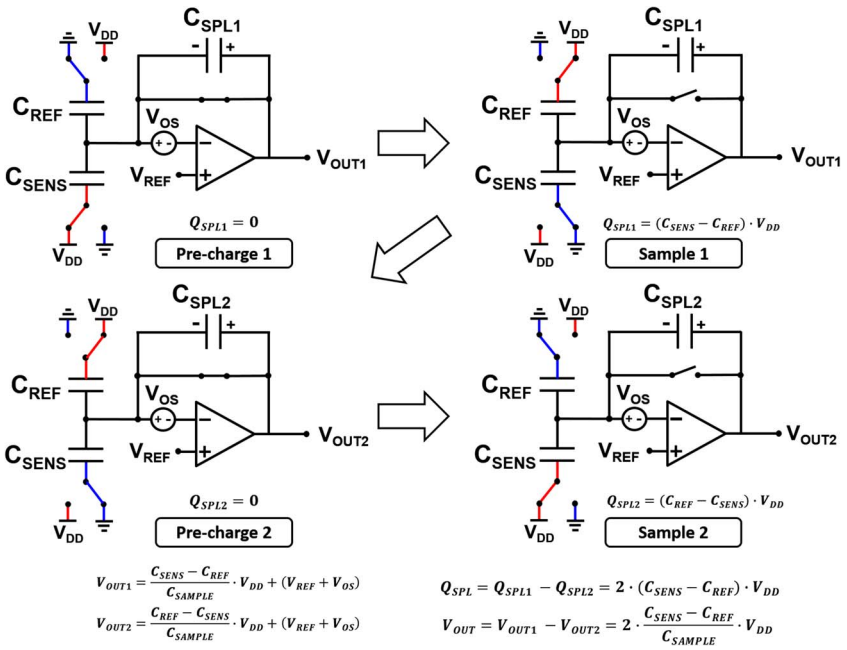

Fig. 19. ***Correlated double-sampling of sensing capacitance in [79].***

FoM of 63.9 fJ per conversion step with 160 nW of power consumption at 250-Hz measurement frequency. Therefore, this CDC could be used in continuous capacitive sensing for systems with a microwatt power budget such as in [48].

E. Low Power Microprocessor

The microprocessor in a WSN plays a critical role of controlling the sensor operation sequence, processing measured data, and managing data storage. Since a microprocessor is an essential element in implementing complex sensor nodes, there has been consistent effort to develop energy-efficient microprocessors. Cortex-M series from ARM is one of the well-known commercial 32-b microprocessor families designed for mobile and sensor applications [80]. Recent demonstration in [81] showed that the Cortex-M0+, the lowest power processor in the Cortex-M family, could achieve 11.7 pJ per instruction with aggressive voltage scaling down to the subthreshold regime and a comprehensive leakage reduction strategy. The retention power for 4 kB of memory and the microprocessor was 80 nW.

Another recent implementation of Cortex-M0+ introduced a new logic family called dynamic leakage-suppression logic (DLSL), which focused on minimizing leakage power consumption rather than optimizing energy per operation [82]. By aggressively suppressing the leakage current during operation, the processor could be slowed down to reduce active time power consumption to as low as 295 pW at 2-Hz operation frequency. This was a power level that could be directly provided by ambient energy harvesters with nanowatt order output power, as shown in Section III-A, enabling a batteryless sensor system.

The details of DLSL are shown in Fig. 20. With a DLSL inverter, the output voltage was fed back to the bottom PMOS (M_{PB}) and the top NMOS (M_{NT}), which acted as power gates for the inverter. When input was 0 V, the pull-down NMOS (M_{NB}) was turned off by the input voltage and the bottom PMOS (M_{PB}) was turned off by the output voltage. Since the two series-connected transistors were turned off, the connecting node ($n2$) settled to roughly half V_{DD}, placing both transistors into super cutoff. This also held when the input was V_{DD} (with a pullup network: M_{NT} and M_{PT}); this makes the leakage of DLSL gates more than two orders of magnitude lower than conventional CMOS logic gates.

For dynamic operations, DLS used leakage currents of top and bottom transistors. When the input of an inverter rose from 0 to V_{DD}, for example, M_{PT} was turned off and M_{NM} was put on weak inversion mode. However, since the initial output was V_{DD}, the output could not be discharged through M_{PB}. But since M_{NB} equates the output voltage and node $n2$, the output voltage dropped and both M_{NT} and M_{PT} were put on super cutoff. At the same time, as the output voltage approached $n2$, M_{PB} was in regular cutoff mode where the leakage current was at least an order of magnitude higher than the top stack transistors in super cutoff, slowly creating a falling output transition. The Cortex-M0+ processor implemented with DLSL could operate with extremely low subnanowatt power at the cost of limited frequency (2–15 Hz).

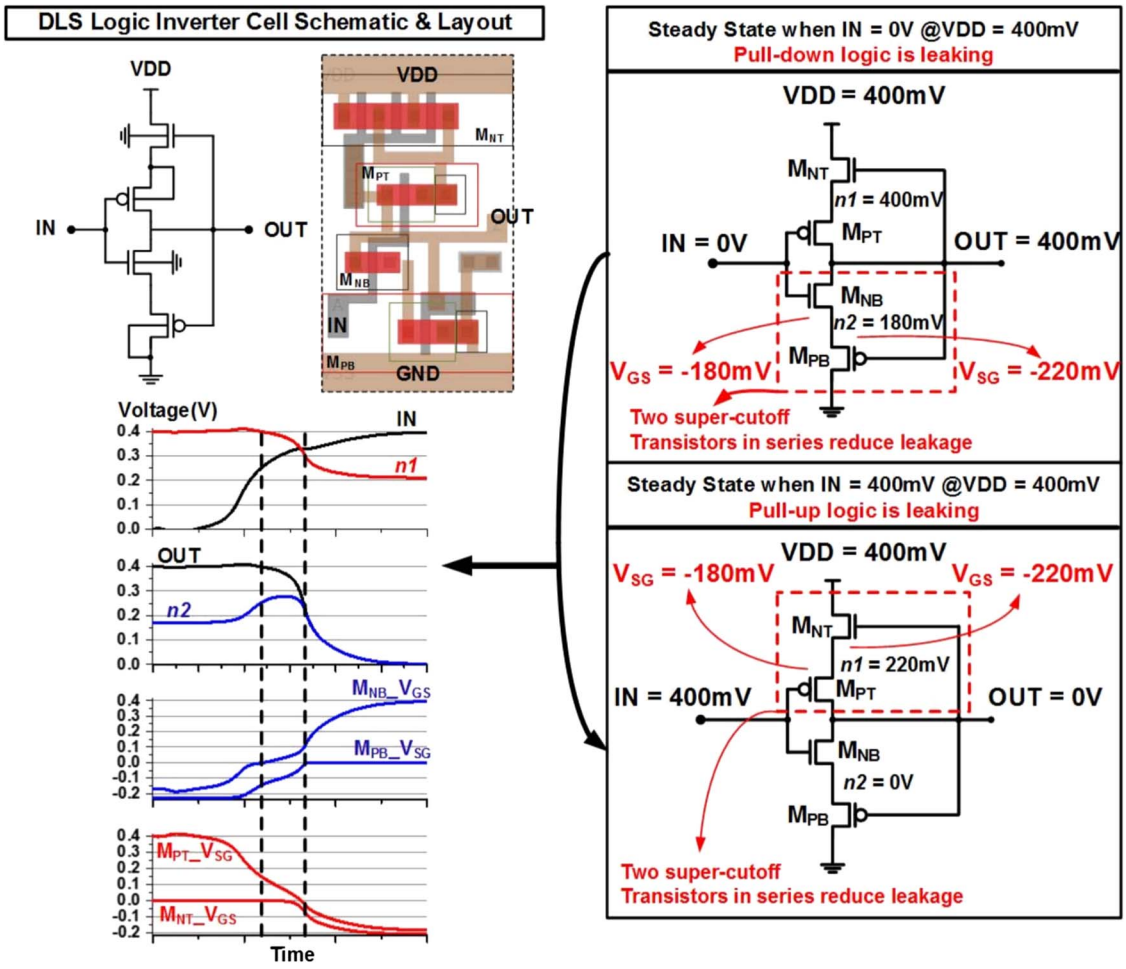

Fig. 20. ***Dynamic leakage suppression logic inverter in [82].***

Hence, for sensor systems with low processing power requirements, it could be an excellent choice for a batteryless system that entirely relies on ambient energy harvesting.

F. Low Power Radio Transmitter

Unlike many other components in a WSN, the radio transmitter is a component for which it is difficult to achieve significant energy efficiency improvement with low power circuit design techniques. This is due to the fact that the base station receiver has a minimum sensitivity level (e.g., −100 dBm) and given the distance and carrier frequency, the path loss is determined and sets the transmit power of the WSN radio. More efficient antenna and transmitter design can reduce the required power to some extent but, obviously, cannot go below a fundamental power level that must be transmitted. A similar limit exists for the WSN receiver where the FCC limit on base station transmit power and the path loss dictate a minimum sensitivity at the WSN, which in turn set the low noise amplifier (LNA) gain and noise figure. For instance, a continuously active UWB radio implemented for small WSNs typically consumed milliwatts of power with nano-Joule (nJ) per bit energy efficiency as shown with [83] and [84] in Table 2. However, for miniature WSN with very small batteries, such as the one in [52], the current in the order of milliamperes sometimes could not be viable due to high internal resistance of the batteries as high as kilohms. To provide the radio transmitter with power greater than the battery can supply, drawing charges from a local reservoir (decoupling capacitor) with a duty-cycled operation is proposed in [85] and [86]. In this scheme, the local reservoir is replenished from the battery after each bit transmission. With a duty-cycling scheme, the radio transmitter was only activated for 100 ns for each bit in [85], achieving 40 μW of power consumption on average, which is acceptable for a small battery with internal resistance of 5 k Ω. Note that energy efficiency is still on the order of nJ per bit. To improve the short distance of the on-chip antenna

TABLE II Low Power Radio Transmitters in Miniature WSNs

	[83]	[84]	[85]	[86]
Type	3.6-4.1GHz UWB	UWB	915MHz UWB on-chip Antenna	8.0GHz UWB Off-chip Antenna
Dimension [mm^3]	40×22×1.1	10×10×10	2×4×4	1.85×4.1×1.4
Active Power	6.75mW	36mW	Avg. 40μW	Avg. 36μW
Standby Power	9μW	1.8μW	15nW	8nW
Distance	60m	10m	15mm	3.8-13.4m
Distance/Volume (Normalized)	0.049	0.0079	0.00037	0.28-1.00
Energy/bit	10.1nJ	3.4nJ	5.3nJ	3.6nJ
Data rate	1kbps	10.7Mbps	7.5kbps	10kbps

in [85], an off-chip antenna was designed to significantly improve the distance with similar power consumption and energy efficiency in [86].

IV. CONCLUSION

WSNs are essential elements supporting a wide range of SHM applications. There has been great progress in the design of small ultralow power WSNs, with emphasis on improving the key metrics of lifetime, power consumption, and total system volume. Recent trends show that energy harvesting has become a popular solution to extend WSN lifetime, with the ultimate goal being energy-autonomous systems. Energy harvesting sources are continuously being diversified, which benefits a broader range of applications. Various sensor node form factors are useful for SHM applications, though generally smaller nodes are preferred. There has been progress in building complete systems as small as a few cubic millimeters using custom-designed ICs. This paper has reviewed recent progress in nanowatt-level energy harvesters, timers, wakeup receivers, sensing modalities, and microprocessors. These are all key building blocks that enable ultralow power WSNs with 10+ year lifetimes, or even batteryless sensor systems with nearly unlimited lifetimes. ■

REFERENCES

[1] K. Maser, R. Egri, A. Lichtenstein, and S. Chase, "Field evaluation of a wireless global bridge evaluation and monitoring system," in *Proc. 11th Conf. Eng. Mech.*, 1996, pp. 955–958.

[2] R. Bennett *et al.*, "Wireless monitoring of highways," *Proc. SPIE—Int. Soc. Opt. Eng.*, vol. 3671, pp. 173–182, 1999.

[3] M. J. S. Lowe, D. N. Alleyne, and P. Cawley, "The mode conversion of guided waves by a part-circumferential notch in a pipe," *J. Appl. Mech.*, vol. 65, no. 3, pp. 649–656, Sep. 1998.

[4] W. E. Daniell and C. A. Taylor, "Effective ambient vibration testing for validating numerical models of concrete dams," *Earthquake Eng. Struct. Dyn.*, vol. 28, no. 11, pp. 1327–1344, 1999.

[5] C. C. Ciang, J.-R. Lee, and H.-J. Bang, "Structural health monitoring for a wind turbine system: A review of damage detection methods," *Meas. Sci. Technol.*, vol. 19, no. 12, 2008.

[6] B. Nejikovsky and E. Keller, "Wireless communications based system to monitor performance of rail vehicles," in *Proc. IEEE/ASME Joint Railroad Conf.*, Newark, NJ, USA, Apr. 4–6, 2000, pp. 111–124.

[7] L. W. Gause, D. G. Krantz, P. J. Biermann, and J. H. Belk, "Early demonstration of remotely queried microsensors," *Proc. SPIE—Int. Soc. Opt. Eng.*, vol. 3673, pp. 190–194, 1999.

[8] P. MacGillivray and K. Goddard, "Advanced sensor technology for marine propulsion control systems," in *Proc. 11th Ship Control Syst. Symp.*, 1997, pp. 245–257.

[9] Y. Liu, S.-B. Kim, A. Chattopadhyay, and D. T. Doyle, "Application of system-identification techniques to health monitoring of on-orbit satellite boom structures," *J. Spacecraft Rockets*, vol. 48, no. 4, pp. 589–598, 2011.

[10] A. Nair and C. S. Cai, "Acoustic emission monitoring of bridges: Review and case studies," *Eng. Struct.*, vol. 32, no. 6, pp. 1704–1714, Jun. 2010.

[11] M. Celebi, "Seismic instrumentation of buildings (with emphasis on federal buildings)", U.S. Geological Survey, Menlo Park, CA, USA, Tech. Rep. 0-7460-68170, 2002.

[12] C. R. Farrar, "Historical overview of structural health monitoring," Los Alamos Dynamics, Los Alamos, NM, USA, Lecture Notes on Structural Health Monitoring Using Statistical Pattern Recognition, 2001.

[13] E. G. Straser and A. S. Kiremidjian, "A modular, wireless damage monitoring system for structures," John A. Blume Earthquake Engineering Center, Stanford Univ., Stanford, CA, USATech. Rep. 128, 1998.

[14] R. Bennett *et al.*, "Wireless monitoring of highways," *Proc. SPIE—Int. Soc. Opt. Eng.*, vol. 3671, pp. 173–182, 1999.

[15] J. P. Lynch *et al.*, "The design of a wireless sensing unit for structural health monitoring," in *Proc. 3rd Int. Workshop Struct. Health Monitor.*, pp. 12–14, Sep. 2001.

[16] M. R. Basheer, V. Rao, and M. Derriso, "Self-organizing wireless sensor networks for structural health monitoring," in *Proc. 4th Int. Workshop Struct. Health Monitor.*, Sep. 2003, pp. 1193–1206.

[17] C. R. Farrar, D. W. Allen, G. Park, S. Ball, and M. P. Masquelier, "Coupling sensing hardware with data interrogation software for structural health monitoring," *Shock and Vibration*, vol. 13, no. 4-5, pp. 519–530, 2006. [Online]. Available: http://dx.doi.org/10.1155/2006/164382

[18] J. P. Lynch *et al.*, "Field validation of a wireless structural health monitoring system on the Alamosa Canyon bridge," *Proc. SPIE—Int. Soc. Opt. Eng.*, vol. 5057, pp. 267–278, Mar. 2004.

[19] J. M. Rabaey, M. J. Ammer, J. L. da Silva, Jr., D. Patel, and S. Roundy, "Pico radio supports *ad hoc* ultra-low power wireless networking," *Computer*, vol. 33, no. 7, pp. 42–48, Jul. 2000.

[20] S. Roundy, D. Steingart, L. Fréchette, P. K. Wright, and J. Rabaey, "Power sources for wireless networks," in *Proc. 1st Eur. Workshop Wireless Sensor Netw.*, 2004, doi: 10.1007/978-3-540-24606-0_1.

[21] E. M. Yeatman, "Advances in power sources for wireless sensor nodes," in *Proc. Int. Workshop Wearable Implantable Body Sensor Netw.*, pp. 20–21, 2004.

[22] P. D. Mitcheson, T. C. Green, E. M. Yeatman, and A. S. Holmes, "Analysis of optimized microgenerator architectures

for self-powered ubiquitous computers," Imperial College Sci. Technol. Med., 2004.

[23] S. Roundy, P. K. Wright, and K. S. Pister, "Micro-electrostatic vibration-to-electricity converters," in *Proc. ASME Int. Mech. Eng. Congr. Expo*, 2002, doi:10.1115/IMECE2002-39309.

[24] A. S. Holmes, "Axial-flow microturbine with electromagnetic generator: Design, CFD simulation, prototype demonstration," in *Proc. 17th IEEE Int. Micro Electro Mech. Syst. Conf.*, 2004, pp. 568–571.

[25] J. Stevens, "Optimized thermal design of small T thermoelectric generators," in *Proc. 34th Intersoc. Energy Conv. Eng. Conf.*, 1999, doi: 10.4271/1999-01-2564.

[26] H.-C. Chung, T. Enotomo, K. Loh, and M. Shinozuka, "Real-time visualization of bridge structural response through wireless MEMS sensors," *Proc. SPIE—Int. Soc. Opt. Eng.*, vol. 5392, pp. 239–246, Mar. 2004.

[27] S. Cho *et al.*, "Structural health monitoring system of a cable-stayed bridge using a dense array of scalable smart sensor network," *Proc. SPIE—Int. Soc. Opt. Eng.*, vol. 7647, Mar. 2010, doi: 10.1117/12.852272.

[28] *Imote2 Hardware Reference Manual*Crossbow, Inc., 2007, Rev. A, PN: 7430-0409-01. [Online]. Available: http://www.xbow.com/Support/Support_pdf_files/Imote2_Hardware_Reference_Manual.pdf

[29] J.-W. Park, H.-J. Jung, H. Jo, S. Jang, and B. F. Spencer Jr., "Feasibility study of wind generator for smart wireless sensor node in cable-stayed bridge," *Proc. SPIE—Int. Soc. Opt. Eng.*, vol. 7647, Apr. 2010, doi: 10.1117/12.853600.

[30] Y. K. Tan and S. K. Panda, "Self-autonomous wireless sensor nodes with wind energy harvesting for remote sensing of wind-driven wildfire spread," *IEEE Trans. Instrum. Meas.*, vol. 60, no. 4, pp. 1367–1377, Apr. 2011.

[31] J. Kymissis, C. Kendall, J. Paradiso, and N. Gershenfeld, "Parasitic power harvesting in shoes," in *Dig. Papers 2nd Int. Symp. Wearable Comput.*, Oct. 1998, pp. 1320–1139.

[32] K. S. Moon, H. Liang, J. Yi, and B. Mika, "Tire tread deformation sensor and energy harvester development for smart-tire applications," *Proc. SPIE—Int. Soc. Opt. Eng.*, vol. 6529, Apr. 2007, doi: 10.1117/12.721009.

[33] T. A. Anderson and D. W. Sexton, "A vibration energy harvesting sensor platform for increased industrial efficiency," *Proc. SPIE—Int. Soc. Opt. Eng.*, vol. 6174, Apr. 2006, doi: 10.1117/12.659586.

[34] J. Li, S. Jang, and J. Tang, "Implementation of a piezoelectric energy harvester in railway health monitoring," *Proc. SPIE—Int. Soc. Opt. Eng.*, vol. 9061, Mar. 2014, doi: 10.1117/12.2045224.

[35] P. Glynne-Jones, M. J. Tudor, S. P. Beeby, and N. M. White, "An electromagnetic, vibration-powered generator for intelligent sensor systems," *Sens. Actuators A, Phys.*, vol. 110, no. 1–3, pp. 344–349, Feb. 2004.

[36] J. Park, S. Kwon, and K. H. Law, "Asynchronous phase shifted electromagnetic energy harvester," *Proc. SPIE—Int. Soc. Opt. Eng.*, vol. 8692, Apr. 2013, doi: 10.1117/12.2009615.

[37] J. Jang, J. F. Liu, C. P. Yue, and H. Sohn, "Development of self-contained sensor skin for highway bridge monitoring," *Proc. SPIE—Int. Soc. Opt. Eng.*, vol. 6174, Apr. 2006, doi: 10.1117/12.659988.

[38] S. G Taylor *et al.*, "A mobile-agent-based wireless sensing network for structural monitoring applications," *Meas. Sci. Technol.*, vol. 20, no. 4, 2009.

[39] S. A. Ouellette and M. D. Todd, "Ultra low-power corrosion-enabled sensor node," *Proc. SPIE—Int. Soc. Opt. Eng.*, vol. 8345, Apr. 2012, doi: 10.1117/12.915290.

[40] J. L. Hill and D. E. Culler, "Mica: A wireless platform for deeply embedded networks," *IEEE Micro*, vol. 22, no. 6, pp. 12–24, Nov./Dec. 2002, doi: 10.1109/MM.2002.1134340.

[41] S.-H. Sim, B. F. Spencer Jr., J. Park, and H. Jung, "Decentralized system identification using stochastic subspace identification on wireless smart sensor networks," *Proc. SPIE—Int. Soc. Opt. Eng.*, vol. 8345, Apr. 2012, doi: 10.1117/12.916126.

[42] M. Saafi and P. Romine, "Embedded MEMS for health monitoring and management of civil infrastructure," *Proc. SPIE—Int. Soc. Opt. Eng.*, vol. 5391, pp. 331–343, Mar. 2004.

[43] M. M. Andringa, J. M. Puryear, D. P. Neikirk, and S. L. Wood, "Low-cost wireless corrosion and conductivity sensors," *Proc. SPIE—Int. Soc. Opt. Eng.*, vol. 6174, Apr. 2006, doi: 10.1117/12.658836.

[44] K. Morita and K. Noguchi, "Crack detection methods for concrete and steel using radio frequency identification and electrically conductive materials and its applications," *Proc. SPIE—Int. Soc. Opt. Eng.*, vol. 6932, Apr. 2008, doi: 10.1117/12.775967.

[45] B. Quinn and G. Kelly, "Feasibility of embedded wireless sensors for monitoring of concrete curing and structural health," *Proc. SPIE—Int. Soc. Opt. Eng.*, vol. 7647, Mar. 2010, doi: 10.1117/12.847529.

[46] X. Xu and H. Huang, "Wireless interrogation of antenna sensors for strain monitoring," *Proc. SPIE—Int. Soc. Opt. Eng.*, vol. 8345, Apr. 2012, doi: 10.1117/12.914977.

[47] H. Huang, "Unpowered wireless generation and sensing of ultrasound," *Proc. SPIE—Int. Soc. Opt. Eng.*, vol. 8692, Apr. 2013, doi: 10.1117/12.2010237.

[48] N. Lajnef, N. Elvin, and S. Chakrabartty, "Piezo-powered floating fate injector for self-powered fatigue monitoring in biomechanical implants," *IEEE Trans. Biomed. Circuits Syst.*, vol. 2, pp. 164–172, Sep. 2008.

[49] C. Huang and S. Chakrabartty, "A miniature batteryless health and usage monitoring system based on hybrid energy harvesting," *Proc. SPIE—Int. Soc. Opt. Eng.*, vol. 7981, Apr. 2011, doi: 10.1117/12.881494.

[50] C. Huang, N. Lajnef, and S. Chakrabartty, "Calibration and characterization of self-powered floating gate usage monitor with single electron per second operational limit," *IEEE Trans. Circuits Syst. I, Reg. Papers*, vol. 57, no. 3, pp. 556–567, Mar. 2010.

[51] Y. Lee *et al.*, "A modular 1 mm^3 die-stacked sensing platform with low power I^2C inter-die communication and multi-modal energy harvesting," *IEEE J. Solid-State Circuits*, vol. 48, no. 1, pp. 229–242, Jan. 2013.

[52] Cymbet Corporation. [Online]. Available: http://www.cymbet.com

[53] W. Jung *et al.*, "An ultra-low power fully integrated energy harvester based on self-oscillating switched-capacitor voltage doubler," *IEEE J. Solid-State Circuits*, vol. 49, no. 12, pp. 2800–2811, Dec. 2014.

[54] S. Oh *et al.*, "Dual-slope capacitance to digital converter integrated in an implantable pressure sensing system," in *Proc. IEEE Eur. Solid-State Circuits Conf.*, Sep. 2014, pp. 295–298.

[55] S. Jeong *et al.*, "A fully-integrated 71 nW CMOS temperature sensor for low power wireless sensor nodes," *IEEE J. Solid-State Circuits*, vol. 49, no. 8, pp. 1682–1693, Aug. 2014.

[56] G. Kim *et al.*, "A millimeter-scale wireless imaging system with continuous motion detection and energy harvesting," in *Symp. VLSI Circuits Dig. Tech. Papers*, Jun. 2014, doi: 10.1109/VLSIC.2014.6858425.

[57] B. Murmann, "ADC performance survey 1997–2015." [Online]. Available: http://web.stanford.edu/~murmann/adcsurvey.html

[58] W. Jung *et al.*, "An ultra-low power fully integrated energy harvester based on self-oscillating switched-capacitor voltage doubler," *IEEE J. Solid-State Circuits*, vol. 49, no. 12, pp. 2800–2811, Dec. 2014.

[59] S. Bandyopadhyay, P. P. Mercier, A. C. Lysaght, K. M. Stankovic, and A. P. Chandrakasan, "A 1.1 nW energy-harvesting system with 544 pW quiescent power for next-generation implants," *IEEE J. Solid-State Circuits*, vol. 49, no. 12, pp. 2812–2824, Dec. 2014.

[60] D. W. Allan, "Statistics of atomic frequency standards," *Proc. IEEE*, vol. 54, no. 2, pp. 221–230, Feb. 1966.

[61] D. Lanfranchi, E. Dijkstra, and D. Aebischer, "A microprocessor-based analog wristwatch chip with 3 seconds/year accuracy," in *Proc. IEEE Int. Solid-State Circuits Conf.*, Feb. 1994, pp. 92–93.

[62] D. Aebischer, H. Oguey, and V. Von Kaenel, "A 2.1 MHz crystal oscillator time base with a current consumption under 500 nA," in *Proc. Eur. Solid-State Circuits Conf.*, Sep. 1996, pp. 60–63.

[63] J.-H. Chang, S. Diao, R. M. Kumarasamy, and M. Je, "32 kHz MEMS-based oscillator for implantable medical devices," in *Proc. Int. Symp. Integr. Circuits*, Dec. 2011, pp. 246–249.

[64] D. Ruffieux, F. Krummenacher, A. Pezous, and G. Spinola-Durante, "Silicon resonator based 3.2 μW real time clock with $\pm$10 ppm frequency accuracy," *IEEE J. Solid-State Circuits*, vol. 45, no. 1, pp. 224–234, Jan. 2010.

[65] D. Yoon, D. Sylvester, and D. Blaauw, "A 5.5 nW 32.768 kHz DLL-assisted XO for real-time clocks in wireless sensing applications," in *Proc. IEEE Int. Solid-State Circuits Conf.*, Feb. 2012, pp. 366–368.

[66] S. Jeong, I. Lee, D. Blaauw, and D. Sylvester, "A 5.8 nW, 45 ppm/°C on-chip CMOS wake-up timer using a constant charge subtraction scheme," in *Proc. Custom Integr. Circuits Conf.*, Sep. 2014, doi: 10.1109/CICC.2014.6946008.

[67] A. Molnar, B. Lu, S. Lanzisera, B. W. Cook, and K. S. J. Pister, "An ultra-low power 900 MHz RF transceiver for wireless sensor networks," in *Proc. IEEE Custom Integr. Circuits Conf.*, 2004, pp. 401–404.

[68] B. W. Cook, A. Berny, A. Molnar, S. Lanzisera, and K. K. K. Pister, "Low-power 2.4-GHz transceiver with passive RX front-end and 400-mV supply," *IEEE J. Solid-State Circuits*, vol. 41, no. 12, pp. 2757–2766, Dec. 2006.

[69] D.-Y. Yoon *et al.*, "A new approach to low-power and low-latency wake-up receiver system for wireless sensor nodes," *IEEE J. Solid-State Circuits*, vol. 47, no. 10, pp. 2405–2419, Oct. 2012.

[70] K. Yadav, I. Kymissis, and P. R. Kinget, "A 4.4- μW wake-up receiver using ultrasound data," *IEEE J. Solid-State Circuits*, vol. 48, no. 3, pp. 649–660, Mar. 2013.

[71] G. Kim *et al.*, "A 695 pW standby power optical wake-up receiver for wireless sensor nodes," in *Proc. IEEE Custom Integr. Circuits Conf.*, Sep. 2012, doi: 10.1109/CICC.2012.6330603.

[72] A. L. Aita, M. A. P. Pertijs, K. A. A. Makinwa, and J. H. Huijsing, "A CMOS smart temperature sensor with a batch-calibrated inaccuracy of $\pm 25°C$ (3σ) from $-70°C$ to 130 °C," in *IEEE ISSCC Dig. Tech. Papers*, Feb. 2009, pp. 342–343.

[73] F. Sebastiano *et al.*, "A 1.2-V 10- W NPN-based temperature sensor in 65-nm CMOS with an inaccuracy of 0.2 °C (3σ) from 70 °C to 125 °C," *IEEE J. Solid-State Circuits*, vol. 45, no. 12, pp. 2591–2601, Dec. 2010.

[74] S. Jeong *et al.*, "A fully-integrated 71 nW CMOS temperature sensor for low power wireless sensor nodes," *IEEE J. Solid-State Circuits*, vol. 49, no. 8, pp. 1682–1693, Aug. 2014.

[75] H. Danneels, K. Coddens, and G. Gielen, "A fully-digital, 0.3 V, 270 nW capacitive sensor interface without external references," in *Proc. ESSCIRC*, 2011, pp. 287–290.

[76] S. Xia, K. Makinwa, and S. Nihtianov, "A capacitance-to-digital converter for displacement sensing with 17 b resolution and 20 μs conversion time," in *ISSCC Dig. Tech. Papers*, Feb. 2012, pp. 198–199.

[77] Z. Tan *et al.*, "A 1.2 V 8.3 nJ energy-efficient CMOS humidity sensor for RFID applications," in *VLSI Circuits Dig. Tech. Papers*, 2012, pp. 24–25.

[78] K. Tanaka, Y. Kuramochi, T. Kurashina, K. Okada, and A. Matsuzawa, "A 0.026 mm^2 capacitance-to-digital converter for biotelemetry applications using a charge redistribution technique," in *Proc. Asian Soild-State Circuits Conf.*, 2007, pp. 244–247.

[79] H. Ha, D. Sylvester, D. Blaauw, and J.-Y. Sim, "A 160 nW 63.9 fJ/conversion-step capacitance-to-digital converter for ultra-low-power wireless sensor nodes," in *Proc. IEEE Int. Solid-State Circuits Conf.*, Feb. 2014, pp. 220–221.

[80] ARM. [Online]. Available: http://www.arm.com/products/processors/cortex-m/

[81] J. Myers *et al.*, "An 80 nW retention 11.7 pJ/cycle active subthreshold ARM Cortex-M0 + subsystem in 65 nm CMOS for WSN applications," in *Proc. Int. Solid- State Circuits Conf.*, Feb. 2015, doi: 10.1109/ISSCC.2015.7062967.

[82] W. Lim, I. Lee, D. Sylvester, and D. Blaauw, "Batteryless sub-nW Cortex-M0 + processor with dynamic leakage-suppression logic," in *Proc. Int. Solid-State Circuits Conf.*, Feb. 2015, doi: 10.1109/ISSCC.2015.7062968.

[83] M. Danesh and J. R. Long, "An autonomous wireless sensor node using a solar cell antenna for solar energy harvesting," in *Microw. Symp. Dig.*, Jun. 2011, doi: 10.1109/MWSYM.2011.5972635.

[84] G. Ono *et al.*, "1-cc computer: Cross-layer integration with 3.4-nW/bps link and 22-cm locationing," in *VLSI Circuits Dig. Tech. Papers*, Jun. 2007, doi: 10.1109/VLSIC.2007.4342778.

[85] G. Kim *et al.*, "A millimeter-scale wireless imaging system with continuous motion detection and energy harvesting," in *VLSI Circuits Dig. Tech. Papers*, Jun. 2014, doi: 10.1109/VLSIC.2014.6858425.

[86] H. Kim *et al.*, "A 10.6 mm^3 fully-integrated, wireless sensor node with 8 GHz UWB transmitter," in *VLSI Circuits Dig. Tech. Papers*, Jun. 2015, doi: 10.1109/VLSIC.2015.7231258.

ABOUT THE AUTHORS

Yoonmyung Lee (Member, IEEE) received the B.S. degree in electronic and electrical engineering from POSTECH, Pohang, Korea, in 2004 and the M.S. and Ph.D. degrees from the University of Michigan, Ann Arbor, MI, USA, in 2008 and 2012, respectively.

During his Ph.D. study, he worked at research labs with Intel Corporation and IBM, exploring novel circuit designs for low power on-die interconnect fabrics and SRAM. He was also a recipient of the Samsung Scholarship and the Intel Ph.D. Fellowship. He has been with the University of Michigan as research faculty since 2012 and joined Sungkyunkwan University, Suwon, Korea, as an Assistant Professor in 2015. His research interests include energy-efficient integrated circuit design for low-power high-performance VLSI systems and millimeter-scale wireless sensor systems.

David Blaauw (Fellow, IEEE) received the B.S. degree in physics and computer science from Duke University, Durham, NC, USA, in 1986 and the Ph.D. degree in computer science from the University of Illinois at Urbana-Champaign, Urbana, IL, USA, in 1991.

After his studies, he worked for Motorola, Inc., Austin, TX, USA, where he was the manager of the High Performance Design Technology group. Since August 2001, he has been on the faculty at the University of Michigan, Ann Arbor, MI, USA, where he is a Professor. He has published over 450 papers and holds 40 patents. His work has focused on VLSI design with particular emphasis on ultralow power and high-performance design.

Dr. Blaauw was the Technical Program Chair and General Chair for the International Symposium on Low Power Electronic and Design. He was also the Technical Program Co-Chair of the ACM/IEEE Design Automation Conference and a member of the ISSCC Technical Program Committee.

Dennis Sylvester (Fellow, IEEE) received the Ph.D. degree in electrical engineering from the University of California Berkeley, Berkeley, CA, USA, where his dissertation was recognized with the David J. Sakrison Memorial Prize as the most outstanding research in the University of California Berkeley Electrical Engineering and Computer Science Department.

He is a Professor of Electrical Engineering and Computer Science at the University of Michigan, Ann Arbor, MI, USA and Director of the Michigan Integrated Circuits Laboratory (MICL), a group of ten faculty and 70+ graduate students. He has held research staff positions in the Advanced Technology Group of Synopsys, Mountain View, CA, USA; Hewlett-Packard Laboratories, Palo Alto, CA; and visiting professorships at the National University of Singapore and Nanyang Technological University. He has published over 400 articles along with one book and several book chapters. His research interests include the design of millimeter-scale computing systems and energy efficient near-threshold computing. He holds 28 U.S. patents. He also serves as a consultant and technical advisory board member for electronic design automation and semiconductor firms in these areas. He cofounded Ambiq Micro, a fabless semiconductor company developing ultralow power mixed-signal solutions for compact wireless devices.

Dr. Sylvester received an NSF CAREER award, the Beatrice Winner Award at ISSCC, an IBM Faculty Award, an SRC Inventor Recognition Award, and nine best paper awards and nominations. He is the recipient of the ACM SIGDA Outstanding New Faculty Award and the University of Michigan Henry Russel Award for distinguished scholarship. He serves on the technical program committee of the IEEE International Solid-State Circuits Conference and previously served on the executive committee of the ACM/IEEE Design Automation Conference. He has served as Associate Editor for the IEEE Transactions on Computer-Aided Design and the IEEE Transactions on very Large Scale Integration (VLSI) Systems and Guest Editor for IEEE Journal of Solid-State Circuits and the IEEE Transactions on Circuits and Systems II: Express Briefs.